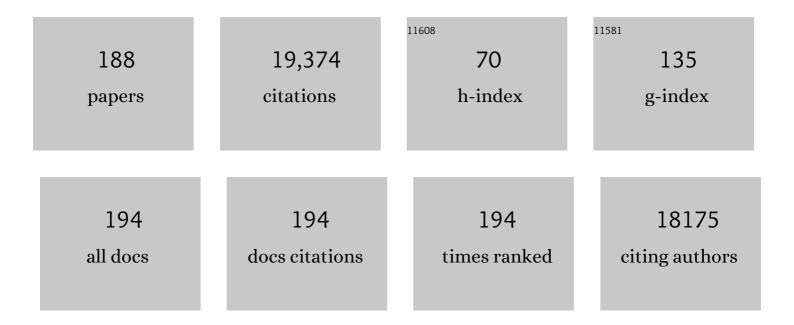
## Matthew D Robson

List of Publications by Year in descending order

Source: https://exaly.com/author-pdf/5220703/publications.pdf Version: 2024-02-01



#	Article	lF	CITATIONS
1	Left Ventricular Non-Compaction. Journal of the American College of Cardiology, 2005, 46, 101-105.	1.2	1,075
2	Myocardial T1 mapping and extracellular volume quantification: a Society for Cardiovascular Magnetic Resonance (SCMR) and CMR Working Group of the European Society of Cardiology consensus statement. Journal of Cardiovascular Magnetic Resonance, 2013, 15, 92.	1.6	864
3	Changes in connectivity profiles define functionally distinct regions in human medial frontal cortex. Proceedings of the National Academy of Sciences of the United States of America, 2004, 101, 13335-13340.	3.3	632
4	Magnetic Resonance: An Introduction to Ultrashort TE (UTE) Imaging. Journal of Computer Assisted Tomography, 2003, 27, 825-846.	0.5	618
5	Shortened Modified Look-Locker Inversion recovery (ShMOLLI) for clinical myocardial T1-mapping at 1.5 and 3 T within a 9 heartbeat breathhold. Journal of Cardiovascular Magnetic Resonance, 2010, 12, 69.	1.6	552
6	Normal Human Left and Right Ventricular and Left Atrial Dimensions Using Steady State Free Precession Magnetic Resonance Imaging. Journal of Cardiovascular Magnetic Resonance, 2005, 7, 775-782.	1.6	527
7	Acquisition and voxelwise analysis of multi-subject diffusion data with Tract-Based Spatial Statistics. Nature Protocols, 2007, 2, 499-503.	5.5	526
8	Noncontrast T1 Mapping for the Diagnosis of Cardiac Amyloidosis. JACC: Cardiovascular Imaging, 2013, 6, 488-497.	2.3	517
9	Identification and Assessment of Anderson-Fabry Disease by Cardiovascular Magnetic Resonance Noncontrast Myocardial T1 Mapping. Circulation: Cardiovascular Imaging, 2013, 6, 392-398.	1.3	399
10	Human non-contrast T1 values and correlation with histology in diffuse fibrosis. Heart, 2013, 99, 932-937.	1.2	390
11	Quantitative Investigation of Connections of the Prefrontal Cortex in the Human and Macaque using Probabilistic Diffusion Tractography. Journal of Neuroscience, 2005, 25, 8854-8866.	1.7	371
12	Non-contrast T1-mapping detects acute myocardial edema with high diagnostic accuracy: a comparison to T2-weighted cardiovascular magnetic resonance. Journal of Cardiovascular Magnetic Resonance, 2012, 14, 53.	1.6	368
13	Multiparametric magnetic resonance for the non-invasive diagnosis of liver disease. Journal of Hepatology, 2014, 60, 69-77.	1.8	367
14	Native T1 Mapping in Transthyretin Amyloidosis. JACC: Cardiovascular Imaging, 2014, 7, 157-165.	2.3	339
15	T1 Mapping for the Diagnosis of Acute Myocarditis Using CMR. JACC: Cardiovascular Imaging, 2013, 6, 1048-1058.	2.3	318
16	Evidence for Microvascular Dysfunction in Hypertrophic Cardiomyopathy. Circulation, 2007, 115, 2418-2425.	1.6	315
17	Myocardial Tissue Characterization Using Magnetic Resonance Noncontrast T1 Mapping in Hypertrophic and Dilated Cardiomyopathy. Circulation: Cardiovascular Imaging, 2012, 5, 726-733.	1.3	286
18	The Evolution of Prefrontal Inputs to the Cortico-pontine System: Diffusion Imaging Evidence from Macaque Monkeys and Humans. Cerebral Cortex, 2006, 16, 811-818.	1.6	258

#	Article	IF	CITATIONS
19	UK Biobank's cardiovascular magnetic resonance protocol. Journal of Cardiovascular Magnetic Resonance, 2016, 18, 8.	1.6	254
20	Between session reproducibility and between subject variability of diffusion MR and tractography measures. NeuroImage, 2006, 33, 867-877.	2.1	245
21	T1 Mapping for Myocardial Extracellular Volume Measurement by CMR. JACC: Cardiovascular Imaging, 2013, 6, 955-962.	2.3	245
22	Effects of High-Dose Modified-Release Nicotinic Acid on Atherosclerosis and Vascular Function. Journal of the American College of Cardiology, 2009, 54, 1787-1794.	1.2	237
23	Cardiovascular magnetic resonance by non contrast T1-mapping allows assessment of severity of injury in acute myocardial infarction. Journal of Cardiovascular Magnetic Resonance, 2012, 14, 15.	1.6	236
24	Normal variation of magnetic resonance T1 relaxation times in the human population at 1.5 T using ShMOLLI. Journal of Cardiovascular Magnetic Resonance, 2013, 15, 13.	1.6	216
25	Dynamic Changes of Edema and Late Gadolinium Enhancement After Acute Myocardial Infarction and Their Relationship to Functional Recovery and Salvage Index. Circulation: Cardiovascular Imaging, 2011, 4, 228-236.	1.3	214
26	Subclinical myocardial inflammation and diffuse fibrosis are common in systemic sclerosis – a clinical study using myocardial T1-mapping and extracellular volume quantification. Journal of Cardiovascular Magnetic Resonance, 2014, 16, 21.	1.6	200
27	Cardiovascular Magnetic Resonance Perfusion Imaging at 3-Tesla for the Detection of Coronary Artery Disease. Journal of the American College of Cardiology, 2007, 49, 2440-2449.	1.2	198
28	Magnetic resonance imaging with ultrashort TE (UTE) PULSE sequences: Technical considerations. Journal of Magnetic Resonance Imaging, 2007, 25, 279-289.	1.9	188
29	Effects of Off-Pump Versus On-Pump Coronary Surgery on Reversible and Irreversible Myocardial Injury. Circulation, 2004, 109, 345-350.	1.6	184
30	Native T1-mapping detects the location, extent and patterns of acute myocarditis without the need for gadolinium contrast agents. Journal of Cardiovascular Magnetic Resonance, 2014, 16, 36.	1.6	184
31	Connectivity-based parcellation of human cortex using diffusion MRI: Establishing reproducibility, validity and observer independence in BA 44/45 and SMA/pre-SMA. NeuroImage, 2007, 34, 204-211.	2.1	182
32	Clinical ultrashort echo time imaging of bone and other connective tissues. NMR in Biomedicine, 2006, 19, 765-780.	1.6	180
33	Beneficial Cardiovascular Effects of Bariatric Surgical and Dietary Weight Loss in Obesity. Journal of the American College of Cardiology, 2009, 54, 718-726.	1.2	176
34	Multiparametric magnetic resonance imaging predicts clinical outcomes in patients with chronic liver disease. Journal of Hepatology, 2016, 64, 308-315.	1.8	170
35	Ectopic and Visceral Fat Deposition inÂLean and Obese Patients With TypeÂ2ÂDiabetes. Journal of the American College of Cardiology, 2016, 68, 53-63.	1.2	165
36	Diffuse Myocardial Fibrosis and Inflammation in Rheumatoid Arthritis. JACC: Cardiovascular Imaging, 2015, 8, 526-536.	2.3	164

#	Article	IF	CITATIONS
37	Measurements of the Temporal fMRI Response of the Human Auditory Cortex to Trains of Tones. NeuroImage, 1998, 7, 185-198.	2.1	160
38	MRI and clinical studies of facial and bulbar muscle involvement in MuSK antibody-associated myasthenia gravis. Brain, 2006, 129, 1481-1492.	3.7	160
39	Magnetic resonance imaging of cortical bone with ultrashort TE pulse sequences. Magnetic Resonance Imaging, 2005, 23, 611-618.	1.0	156
40	Reproducibility of native myocardial T1 mapping in the assessment of Fabry disease and its role in early detection of cardiac involvement by cardiovascular magnetic resonance. Journal of Cardiovascular Magnetic Resonance, 2014, 16, 99.	1.6	154
41	Multiparametric magnetic resonance imaging for the assessment of nonâ€alcoholic fatty liver disease severity. Liver International, 2017, 37, 1065-1073.	1.9	145
42	Measurement of the point spread function in MRI using constant time imaging. Magnetic Resonance in Medicine, 1997, 38, 733-740.	1.9	142
43	Noncontrast myocardial <i>T</i> <sub>1</sub> mapping using cardiovascular magnetic resonance for iron overload. Journal of Magnetic Resonance Imaging, 2015, 41, 1505-1511.	1.9	139
44	Pheochromocytoma Is Characterized byÂCatecholamine-Mediated Myocarditis, Focal and Diffuse Myocardial Fibrosis, andÂMyocardial Dysfunction. Journal of the American College of Cardiology, 2016, 67, 2364-2374.	1.2	139
45	<i>T</i> <sub>1</sub> measurements in the human myocardium: The effects of magnetization transfer on the SASHA and MOLLI sequences. Magnetic Resonance in Medicine, 2013, 70, 664-670.	1.9	135
46	Molecular MRI enables early and sensitive detection of brain metastases. Proceedings of the National Academy of Sciences of the United States of America, 2012, 109, 6674-6679.	3.3	131
47	Automatic Measurement of the MyocardialÂInterstitium. JACC: Cardiovascular Imaging, 2016, 9, 54-63.	2.3	127
48	Cardiac energetics, oxygenation, and perfusion during increased workload in patients with type 2 diabetes mellitus. European Heart Journal, 2016, 37, 3461-3469.	1.0	124
49	Myocardial Tissue Characterization by Magnetic Resonance Imaging. Journal of Thoracic Imaging, 2014, 29, 147-154.	0.8	122
50	Magic angle effects in MR neurography. American Journal of Neuroradiology, 2004, 25, 431-40.	1.2	122
51	Global impairment of brachial, carotid, and aortic vascular function in young smokers. Journal of the American College of Cardiology, 2004, 44, 2056-2064.	1.2	119
52	Global Improvement of Vascular Function and Redox State With Low-Dose Folic Acid. Circulation, 2007, 115, 2262-2270.	1.6	119
53	Adenosine Stress and Rest T1 Mapping Can Differentiate Between Ischemic, Infarcted, Remote, and Normal Myocardium Without the Need for Gadolinium Contrast Agents. JACC: Cardiovascular Imaging, 2016, 9, 27-36.	2.3	118
54	Effects of Catecholamine Stress on Diastolic Function and Myocardial Energetics in Obesity. Circulation, 2012, 125, 1511-1519.	1.6	117

#	Article	lF	CITATIONS
55	Differentiation of Athlete's Heart from Pathological Forms of Cardiac Hypertrophy by Means of Geometric Indices Derived from Cardiovascular Magnetic Resonance. Journal of Cardiovascular Magnetic Resonance, 2005, 7, 551-558.	1.6	115
56	Magnetic resonance imaging of the Achilles tendon using ultrashort TE (UTE) pulse sequences. Clinical Radiology, 2004, 59, 727-735.	0.5	107
57	Human cardiac <sup>31</sup> P magnetic resonance spectroscopy at 7 tesla. Magnetic Resonance in Medicine, 2014, 72, 304-315.	1.9	100
58	Myocardial Tissue Phase Mapping with Cine Phase-Contrast MR Imaging: Regional Wall Motion Analysis in Healthy Volunteers. Radiology, 2006, 238, 816-826.	3.6	94
59	Multiple Inflow Pulsed Arterial Spin-Labeling Reveals Delays in the Arterial Arrival Time in Minor Stroke and Transient Ischemic Attack. American Journal of Neuroradiology, 2010, 31, 1892-1894.	1.2	93
60	Relationship Between Regional Myocardial Oxygenation and Perfusion in Patients With Coronary Artery Disease. Circulation: Cardiovascular Imaging, 2010, 3, 32-40.	1.3	92
61	MRI of the brain with ultra-short echo-time pulse sequences. Neuroradiology, 2003, 45, 887-892.	1.1	91
62	Diffusion-weighted multiple shot echo planar imaging of humans without navigation. Magnetic Resonance in Medicine, 1997, 38, 82-88.	1.9	90
63	Identification of Myocardial Disarray inÂPatients With HypertrophicÂCardiomyopathy and Ventricular Arrhythmias. Journal of the American College of Cardiology, 2019, 73, 2493-2502.	1.2	88
64	Addressing a systematic vibration artifact in diffusionâ€weighted MRI. Human Brain Mapping, 2010, 31, 193-202.	1.9	85
65	Determination of cardiac volumes and mass with FLASH and SSFP cine sequences at 1.5 vs. 3 Tesla: A validation study. Journal of Magnetic Resonance Imaging, 2006, 24, 312-318.	1.9	81
66	Evidence for a vascular contribution to diffusion FMRI at high <i>b</i> value. Proceedings of the National Academy of Sciences of the United States of America, 2007, 104, 20967-20972.	3.3	81
67	Myocardial Oxygenation in Coronary Artery Disease. Journal of the American College of Cardiology, 2012, 59, 1954-1964.	1.2	77
68	OXSA: An open-source magnetic resonance spectroscopy analysis toolbox in MATLAB. PLoS ONE, 2017, 12, e0185356.	1.1	77
69	Arterial Effects of Canakinumab in PatientsÂWith Atherosclerosis and TypeÂ2ÂDiabetes or Glucose Intolerance. Journal of the American College of Cardiology, 2016, 68, 1769-1780.	1.2	75
70	Black-Blood Multicontrast Imaging of Carotid Arteries with DANTE-prepared 2D and 3D MR Imaging. Radiology, 2014, 273, 560-569.	3.6	74
71	Magnetic resonance imaging of the knee with ultrashort TE pulse sequences. Magnetic Resonance Imaging, 2004, 22, 1061-1067.	1.0	73
72	Partial fourier partially parallel imaging. Magnetic Resonance in Medicine, 2005, 53, 1393-1401.	1.9	73

#	Article	IF	CITATIONS
73	CMR Native T1 Mapping Allows Differentiation of Reversible Versus Irreversible Myocardial Damage in ST-Segment–Elevation Myocardial Infarction. Circulation: Cardiovascular Imaging, 2017, 10, .	1.3	71
74	Connectivity of the human periventricular—periaqueductal gray region. Journal of Neurosurgery, 2005, 103, 1030-1034.	0.9	70
75	Receive array magnetic resonance spectroscopy: Whitened singular value decomposition (WSVD) gives optimal Bayesian solution. Magnetic Resonance in Medicine, 2010, 63, 881-891.	1.9	67
76	Accelerated human cardiac diffusion tensor imaging using simultaneous multislice imaging. Magnetic Resonance in Medicine, 2015, 73, 995-1004.	1.9	67
77	Myocardial perfusion and oxygenation are impaired during stress in severe aortic stenosis and correlate with impaired energetics and subclinical left ventricular dysfunction. Journal of Cardiovascular Magnetic Resonance, 2014, 16, 29.	1.6	65
78	Rapid quantification of myocardial lipid content in humans using single breathâ€hold 1 H MRS at 3 Tesla. Magnetic Resonance in Medicine, 2011, 66, 619-624.	1.9	64
79	A model for hepatic fibrosis: the competing effects of cell loss and iron on shortened modified Look-Locker inversion recovery <i>T</i> <sub>1</sub> (shMOLLI- <i>T</i> <sub>1</sub> ) in the liver. Journal of Magnetic Resonance Imaging, 2017, 45, 450-462.	1.9	64
80	Plaque Features Associated With Increased Cerebral Infarction After Minor Stroke and TIA. JACC: Cardiovascular Imaging, 2012, 5, 388-396.	2.3	60
81	Quantification of Lipid-Rich Core in Carotid Atherosclerosis Using Magnetic Resonance T2ÂMapping. JACC: Cardiovascular Imaging, 2017, 10, 747-756.	2.3	60
82	Phase contrast ultrashort TE: A more reliable technique for measurement of highâ€velocity turbulent stenotic jets. Magnetic Resonance in Medicine, 2009, 62, 626-636.	1.9	59
83	Anti-TNF modulation reduces myocardial inflammation and improves cardiovascular function in systemic rheumatic diseases. International Journal of Cardiology, 2018, 270, 253-259.	0.8	58
84	Human imaging of phosphorus in cortical and trabecular bone in vivo. Magnetic Resonance in Medicine, 2004, 51, 888-892.	1.9	55
85	Ultrashort TE chemical shift imaging (UTE-CSI). Magnetic Resonance in Medicine, 2005, 53, 267-274.	1.9	55
86	In-vivo quantitative T2 mapping of carotid arteries in atherosclerotic patients: segmentation and T2 measurement of plaque components. Journal of Cardiovascular Magnetic Resonance, 2013, 15, 69.	1.6	55
87	Systolic ShMOLLI myocardial T1-mapping for improved robustness to partial-volume effects and applications in tachyarrhythmias. Journal of Cardiovascular Magnetic Resonance, 2015, 17, 77.	1.6	55
88	Aortic 4D flow: Quantification of signal-to-noise ratio as a function of field strength and contrast enhancement for 1.5T, 3T, and 7T. Magnetic Resonance in Medicine, 2015, 73, 1864-1871.	1.9	55
89	Assessment of Left Atrial Volumes at 1.5 Tesla and 3 Tesla Using FLASH and SSFP Cine Imaging. Journal of Cardiovascular Magnetic Resonance, 2007, 9, 673-679.	1.6	54
90	Early changes in arterial structure and function following statin initiation: Quantification by magnetic resonance imaging. Atherosclerosis, 2008, 197, 951-958.	0.4	54

#	Article	IF	CITATIONS
91	A consistent relationship between local white matter architecture and functional specialisation in medial frontal cortex. NeuroImage, 2006, 30, 220-227.	2.1	53
92	Blunted Myocardial Oxygenation Response During Vasodilator Stress in Patients With Hypertrophic Cardiomyopathy. Journal of the American College of Cardiology, 2013, 61, 1169-1176.	1.2	53
93	Influence of fat on liver <i>T</i> <sub>1</sub> measurements using modified Look–Locker inversion recovery (MOLLI) methods at 3T. Journal of Magnetic Resonance Imaging, 2016, 44, 105-111.	1.9	51
94	Diagnostic Value of Pre-Contrast T1 Mapping in Acute and Chronic Myocardial Infarction. JACC: Cardiovascular Imaging, 2013, 6, 739-742.	2.3	50
95	Quantitative ultrashort echo time imaging for assessment of massive iron overload at 1.5 and 3 Tesla. Magnetic Resonance in Medicine, 2017, 78, 1839-1851.	1.9	50
96	Reducing distortions in diffusionâ€weighted echo planar imaging with a dualâ€echo blipâ€reversed sequence. Magnetic Resonance in Medicine, 2010, 64, 382-390.	1.9	49
97	Simultaneous assessment of cardiac metabolism and perfusion using copolarized [1â€ <sup>13</sup> C]pyruvate and <sup>13</sup> Câ€urea. Magnetic Resonance in Medicine, 2017, 77, 151-1	58 <mark>1.9</mark>	47
98	Quantitative imaging of magnetization transfer using multiple selective pulses. Magnetic Resonance in Medicine, 1999, 41, 1065-1072.	1.9	46
99	Functional and Structural Vascular Remodeling in Elite Rowers Assessed by Cardiovascular Magnetic Resonance. Journal of the American College of Cardiology, 2006, 48, 790-797.	1.2	44
100	Sex-specific characteristics of cardiac function, geometry, and mass in young adult elite athletes. Journal of Magnetic Resonance Imaging, 2006, 24, 297-303.	1.9	44
101	Coil combination for receive array spectroscopy: Are dataâ€driven methods superior to methods using computed field maps?. Magnetic Resonance in Medicine, 2016, 75, 473-487.	1.9	44
102	Contrast enhancement of short T2 tissues using ultrashort TE (UTE) pulse sequences. Clinical Radiology, 2004, 59, 720-726.	0.5	43
103	Cardiovascular Magnetic Resonance Imaging for Non-Invasive Assessment of Vascular Function: Validation against Ultrasound. Journal of Cardiovascular Magnetic Resonance, 2006, 8, 381-387.	1.6	43
104	Inversion recovery at 7 T in the human myocardium: Measurement of <i>T</i> <sub>1</sub> , inversion efficiency and <i>B</i> <sub>1</sub> <sup>+</sup> . Magnetic Resonance in Medicine, 2013, 70, 1038-1046.	1.9	39
105	Cardiac perfusion imaging using hyperpolarized <sup>13</sup> c urea using flow sensitizing gradients. Magnetic Resonance in Medicine, 2016, 75, 1474-1483.	1.9	39
106	Multi-modal magnetic resonance imaging quantifies atherosclerosis and vascular dysfunction in patients with type 2 diabetes mellitus. Diabetes and Vascular Disease Research, 2007, 4, 44-48.	0.9	38
107	Longitudinally and circumferentially directed movements of the left ventricle studied by cardiovascular magnetic resonance phase contrast velocity mapping. Journal of Cardiovascular Magnetic Resonance, 2010, 12, 48.	1.6	38
108	Quantitative magnetization transfer ultrashort echo time imaging of the Achilles tendon. Magnetic Resonance in Medicine, 2011, 65, 1372-1376.	1.9	38

#	Article	IF	CITATIONS
109	A comparison of cardiac <sup>31</sup> P MRS at 1.5 and 3 T. NMR in Biomedicine, 2008, 21, 793-798.	1.6	37
110	Mapping tissue water <i>T</i> <sub>1</sub> in the liver using the MOLLI <i>T</i> <sub>1</sub> method in the presence of fat, iron and <i>B</i> <sub>0</sub> inhomogeneity. NMR in Biomedicine, 2019, 32, e4030.	1.6	37
111	Influence of Contrast Agent Dose and Image Acquisition Timing on the Quantitative Determination of Nonviable Myocardial Tissue Using Delayed Contrast?Enhanced Magnetic Resonance Imaging. Journal of Cardiovascular Magnetic Resonance, 2004, 6, 541-548.	1.6	36
112	Measuring inorganic phosphate and intracellular pH in the healthy and hypertrophic cardiomyopathy hearts by in vivo 7T 31P-cardiovascular magnetic resonance spectroscopy. Journal of Cardiovascular Magnetic Resonance, 2019, 21, 19.	1.6	35
113	A combined analysis and magnetic resonance imaging technique for computerised automatic measurement of cartilage thickness in the distal interphalangeal joint. Magnetic Resonance Imaging, 1995, 13, 709-718.	1.0	34
114	Using a whole-body 31P birdcage transmit coil and 16-element receive array for human cardiac metabolic imaging at 7T. PLoS ONE, 2017, 12, e0187153.	1.1	34
115	Cardiac Cine MR-Imaging at 3T: FLASH vs SSFP. Journal of Cardiovascular Magnetic Resonance, 2006, 8, 709-715.	1.6	32
116	No Evidence of Myocardial Oxygen Deprivation in Nonischemic Heart Failure. Circulation: Heart Failure, 2015, 8, 1088-1093.	1.6	31
117	Dilated Cardiomyopathy: Phosphorus 31 MR Spectroscopy at 7 T. Radiology, 2016, 281, 409-417.	3.6	31
118	Three-dimensional strain-rate imaging. Magnetic Resonance in Medicine, 1996, 36, 537-546.	1.9	30
119	Magnetic resonance imaging of facial muscles. Clinical Radiology, 2007, 62, 1078-1086.	0.5	29
120	Irreversible Myocardial Injury: Assessment with Cardiovascular Delayed-Enhancement MR Imaging and Comparison of 1.5 and 3.0 T—Initial Experience. Radiology, 2007, 242, 735-742.	3.6	27
121	Comparison of two ultrashort echo time sequences for the quantification of <i>T</i> <sub>1</sub> within phantom and human Achilles tendon at 3 T. Magnetic Resonance in Medicine, 2012, 68, 1279-1284.	1.9	27
122	Non-invasive assessment of portal hypertension by multi-parametric magnetic resonance imaging of the spleen: A proof of concept study. PLoS ONE, 2019, 14, e0221066.	1.1	27
123	Reconstruction as a source of artifact in nongated single-shot diffusion-weighted EPI. Magnetic Resonance Imaging, 2005, 23, 899-905.	1.0	26
124	TREMR: Tableâ€resonance elastography with MR. Magnetic Resonance in Medicine, 2009, 62, 815-821.	1.9	26
125	Automated localization and quality control of the aorta in cine CMR can significantly accelerate processing of the UK Biobank population data. PLoS ONE, 2019, 14, e0212272.	1.1	26
126	Imaging of the Achilles tendon in spondyloarthritis: a comparison of ultrasound and conventional, short and ultrashort echo time MRI with and without intravenous contrast. European Radiology, 2011, 21, 1144-1152.	2.3	25

#	Article	IF	CITATIONS
127	Phosphodiester content measured in human liver by in vivo <sup>31</sup> P MR spectroscopy at 7 tesla. Magnetic Resonance in Medicine, 2017, 78, 2095-2105.	1.9	25
128	T2 mapping MRI technique quantifies carotid plaque lipid, and its depletion after statin initiation, following acute myocardial infarction. Atherosclerosis, 2018, 279, 100-106.	0.4	25
129	Detection and monitoring of progressive degeneration of osteoarthritic cartilage by MRI. Acta Orthopaedica, 1995, 66, 130-138.	1.4	25
130	Evidence of a Direct Effect of Myocardial Steatosis on LV Hypertrophy and Diastolic Dysfunction in Adult and Adolescent Obesity. JACC: Cardiovascular Imaging, 2015, 8, 1468-1470.	2.3	23
131	Reproducibility and accuracy of automated measurement for dynamic arterial lumen area by cardiovascular magnetic resonance. International Journal of Cardiovascular Imaging, 2009, 25, 797-808.	0.7	21
132	Quantification of carotid plaque lipid content with magnetic resonance T2 mapping in patients undergoing carotid endarterectomy. PLoS ONE, 2017, 12, e0181668.	1.1	21
133	Computerised planning of the acquisition of cardiac MR images. Computerized Medical Imaging and Graphics, 2004, 28, 411-418.	3.5	20
134	Investigating a Liver Fat. Arteriosclerosis, Thrombosis, and Vascular Biology, 2016, 36, 198-203.	1.1	20
135	Blochâ€Siegert â€mapping for human cardiac <sup>31</sup> Pâ€MRS at 7 Tesla. Magnetic Resonance in Medicine, 2016, 76, 1047-1058.	1.9	18
136	The relationship of perivascular adipose tissue and atherosclerosis in the aorta and carotid arteries, determined by magnetic resonance imaging. Diabetes and Vascular Disease Research, 2018, 15, 286-293.	0.9	18
137	Creatine kinase rate constant in the human heart measured with 3 <scp>D</scp> â€localization at 7 tesla. Magnetic Resonance in Medicine, 2017, 78, 20-32.	1.9	17
138	Consequences of T 2 relaxation during halfâ€pulse slice selection for ultrashort TE imaging. Magnetic Resonance in Medicine, 2010, 64, 610-615.	1.9	16
139	Automated tuning of an eightâ€channel cardiac transceive array at 7 tesla using piezoelectric actuators. Magnetic Resonance in Medicine, 2015, 73, 2390-2397.	1.9	16
140	31P cardiac magnetic resonance spectroscopy during leg exercise at 3 Tesla. International Journal of Cardiovascular Imaging, 2009, 25, 819-826.	0.7	15
141	Loss of fine structure and edge sharpness in fastâ€spinâ€echo carotid wall imaging: Measurements and comparison with multipleâ€spinâ€echo in normal and atherosclerotic subjects. Journal of Magnetic Resonance Imaging, 2011, 33, 1136-1143.	1.9	13
142	Normal values of regional and global myocardial wall motion in young and elderly individuals using navigator gated tissue phase mapping. Age, 2014, 36, 231-241.	3.0	13
143	Optimized saturation pulse train for human firstâ€pass myocardial perfusion imaging at 7T. Magnetic Resonance in Medicine, 2015, 73, 1450-1456.	1.9	13
144	Large dynamic range relative B1+ mapping. Magnetic Resonance in Medicine, 2016, 76, 490-499.	1.9	13

#	Article	IF	CITATIONS
145	Diaphragm position can be accurately estimated from the scattering of a parallel transmit RF coil at 7 T. Magnetic Resonance in Medicine, 2018, 79, 2164-2169.	1.9	13
146	Hypertrophic cardiomyopathy in Noonan Syndrome closely mimics familial hypertrophic cardiomyopathy due to sarcomeric mutations. International Journal of Cardiovascular Imaging, 2006, 22, 493-495.	0.7	12
147	Suppression of skeletal muscle signal using a crusher coil: A human cardiac 31 pâ€MR spectroscopy study at 7 tesla. Magnetic Resonance in Medicine, 2016, 75, 962-972.	1.9	12
148	Accuracy of Quantitative MR Vessel Wall Imaging Applying a Semi?Automated Gradient Detection Algorithm?A Validation Study. Journal of Cardiovascular Magnetic Resonance, 2004, 6, 895-907.	1.6	11
149	A look-locker acquisition scheme for quantitative myocardial perfusion imaging with FAIR arterial spin labeling in humans at 3 tesla. Magnetic Resonance in Medicine, 2017, 78, 541-549.	1.9	11
150	Adiabatic excitation for <sup>31</sup> P MR spectroscopy in the human heart at 7 T: A feasibility study. Magnetic Resonance in Medicine, 2017, 78, 1667-1673.	1.9	11
151	Visualization of the Ruptured Plaque by Magnetic Resonance Imaging. Circulation, 2003, 108, 2542-2542.	1.6	10
152	Multimodal cardiovascular magnetic resonance quantifies regional variation in vascular structure and function in patients with coronary artery disease: Relationships with coronary disease severity. Journal of Cardiovascular Magnetic Resonance, 2011, 13, 61.	1.6	10
153	Feasibility of absolute quantification for 31 P MRS at 7 T. Magnetic Resonance in Medicine, 2019, 82, 49-61.	1.9	10
154	Effects of steady state free precession parameters on cardiac mass, function, and volumes. International Journal of Cardiovascular Imaging, 2007, 23, 583-589.	0.7	9
155	Cardiovascular Magnetic Resonance: Physics and Terminology. Progress in Cardiovascular Diseases, 2011, 54, 181-190.	1.6	9
156	Quantifying sclerotic bone metastases with 2D ultra short TE MRI: A feasibility study. Cancer Biomarkers, 2011, 7, 211-218.	0.8	9
157	Age and gender dependence of pre-contrast T1-relaxation times in normal human myocardium at 1.5T using ShMOLLI. Journal of Cardiovascular Magnetic Resonance, 2012, 14, .	1.6	9
158	Quantitative MRI measurements of the Achilles tendon in spondyloarthritis using ultrashort echo times. British Journal of Radiology, 2012, 85, e293-e299.	1.0	8
159	Non-invasive imaging of carotid arterial restenosis using 3T cardiovascular magnetic resonance. Journal of Cardiovascular Magnetic Resonance, 2014, 16, 5.	1.6	8
160	Chasing the reflected wave back into the heart: a new hypothesis while the jury is still out. Vascular Health and Risk Management, 2011, 7, 365.	1.0	7
161	Microscopic magnetic resonance imaging reveals high prevalence of third coronary artery in human and rabbit heart. Europace, 2012, 14, v73-v81.	0.7	7
162	Hexagonal gradient scheme with RF spoiling improves spoiling performance for highâ€flipâ€angle fast gradient echo imaging. Magnetic Resonance in Medicine, 2017, 77, 1231-1237.	1.9	7

#	Article	IF	CITATIONS
163	Cardiac gating using scattering of an 8â€channel parallel transmit coil at 7T. Magnetic Resonance in Medicine, 2018, 80, 633-640.	1.9	7
164	Hydration and glycogen affect T <sub>1</sub> relaxation times of liver tissue. NMR in Biomedicine, 2021, 34, e4530.	1.6	7
165	Quantification of acute myocardial injury by ShMOLLI T1-Mapping, T2-weighted and late gadolinium imaging in patients presenting with chest pain, positive troponins and non-obstructive coronary arteries. Journal of Cardiovascular Magnetic Resonance, 2011, 13, .	1.6	6
166	Histological validation of ShMOLLI equilibrium contrast CMR for the measurement of diffuse myocardial fibrosis. Journal of Cardiovascular Magnetic Resonance, 2012, 14, .	1.6	6
167	Highly trabeculated structure of the human endocardium underlies asymmetrical response to low-energy monophasic shocks. Chaos, 2017, 27, 093913.	1.0	6
168	Navigatorâ€based reacquisition and estimation of motionâ€corrupted data: Application to multiâ€echo spin echo for carotid wall MRI. Magnetic Resonance in Medicine, 2020, 83, 2026-2041.	1.9	6
169	Scattering matrix imaging pulse design for realâ€time respiration and cardiac motion monitoring. Magnetic Resonance in Medicine, 2019, 82, 2169-2177.	1.9	5
170	Emerging artificial intelligence applications in liver magnetic resonance imaging. World Journal of Gastroenterology, 2021, 27, 6825-6843.	1.4	5
171	Pre-contrast ShMOLLI T1 mapping in cardiac AL amyloidosis. Journal of Cardiovascular Magnetic Resonance, 2012, 14, .	1.6	4
172	In-vivo T2 mapping of atherosclerotic plaques in carotid arteries. Journal of Cardiovascular Magnetic Resonance, 2012, 14, .	1.6	2
173	The diagnostic performance of non-contrast T1-mapping in patients with acute myocarditis on cardiovascular magnetic resonance imaging. Journal of Cardiovascular Magnetic Resonance, 2012, 14, .	1.6	2
174	T1-mapping accurately detects acute myocardial edema: a comparison to T2-weighted cardiovascular magnetic resonance imaging. Journal of Cardiovascular Magnetic Resonance, 2012, 14, .	1.6	2
175	Reply to: "Multiparametric magnetic resonance imaging to predict clinical outcomes in patients with chronic liver disease: A cautionary note on a promising technique― Journal of Hepatology, 2017, 66, 457-458.	1.8	2
176	A 'broken heart' artifact in cardiovascular MR. International Journal of Cardiovascular Imaging, 2003, 19, 437-437.	0.2	1
177	Magnetic resonance phase contrast velocity mapping for flow quantification in irregular heart rhythms using radial k-space ultrashort echo time imaging. International Journal of Cardiology, 2020, 317, 211-215.	0.8	1
178	Cardiovascular Magnetic Resonance: Basic Principles, Methods and Techniques. , 0, , 28-68.		0
179	Evaluation of 3-dimensional left ventricular velocities with cardiac MR imaging using navigator gated high temporal resolution tissue phase mapping. Journal of Cardiovascular Magnetic Resonance, 2009, 11, .	1.6	0
180	Evaluation of left ventricular wall motion in ischaemic heart disease pre- and post-cardiac surgery using cardiac MR. Journal of Cardiovascular Magnetic Resonance, 2010, 12, .	1.6	0

#	Article	IF	CITATIONS
181	Non-contrast T1 mapping characterizes the myocardium beyond that achieved by late gadolinium enhancement in both hypertrophic and dilated cardiomyopathy. Journal of Cardiovascular Magnetic Resonance, 2012, 14, .	1.6	0
182	Single breath-hold Vd(m) calculation as good as multi breath-hold technique in Equilibrium Contrast CMR. Journal of Cardiovascular Magnetic Resonance, 2012, 14, .	1.6	0
183	Response to Letter Regarding Article, "Myocardial Tissue Characterization Using Magnetic Resonance Noncontrast T1 Mapping in Hypertrophic and Dilated Cardiomyopathy― Circulation: Cardiovascular Imaging, 2013, 6, e2.	1.3	0
184	Systolic ShMOLLI T1-mapping is feasible in tachyarrhythmia, with improved image quality compared to diastolic readout. Journal of Cardiovascular Magnetic Resonance, 2015, 17, Q5.	1.6	0
185	6â€Diffusion tensor magnetic resonance imaging of myocardial disarray in hypertrophic cardiomyopathy. , 2018, , .		0
186	Plaque and Wall Assessment. , 2010, , 334-346.		0
187	Abstract 15822: Phosphorus Magnetic Resonance Spectroscopy is More Precise at 7 Tesla Field Strength Than 3 Tesla in Patients With Dilated Cardiomyopathy. Circulation, 2015, 132, .	1.6	0
188	1â€Carotid plaque lipid reduction, determined by T2 mapping, occurs early after high-intensity statin initiation in patients presented with acute myocardial infarction. , 2018, , .		0